Numerical Evaluation of Cable Earth Return Impedance through a Reliable Algorithm based on a Taylor-Series Expansion

R. Iracheta, and N. Flores-Guzman

***Abstract*-- In this paper is proposed an efficient and accurate algorithmic solution based on a Taylor-Series expansion for evaluating the earth return impedance on buried cables. This algorithm solution uses the analysis made by Wedepohl and Wilcox's to transform the Pollaczek's integral into a set of Bessel functions plus a definite integral. The main feature of Bessel functions is that they are easy to compute in modern mathematical tools such as Matlab®. However, the definite integral is approximated by an infinite series, since it does not have analytical solution. The accuracy and efficiency of the proposed method is compared against the numerical integration method for a broad ranges and cable configurations through the criterion of percent absolute error and 3D graphs. Finally, the proposed algorithm is used as a subroutine for cable parameter calculation of the inverse Numerical Laplace Transform (NLT) to obtain accurate transient responses in the time domain.**

***Keywords*: Earth-return impedance, Pollazcek's integral, Wedepohl's integral, Taylor series expansion, buried cables.**

I. Introduction

The accurate calculation of the earth return impedance ($\boldsymbol{Z_T}$) parameter is extremely important for modeling transmission lines and cables as well as, to perform reliable analysis of electromagnetic transients and electromagnetic compatibility. The most important expressions to evaluate $\boldsymbol{Z_T}$ have been first published by Carson in 1926 for aerial lines and later by Pollaczek for buried cables and combination of buried cables and overhead conductors [1-2]. These formulations are represented by a set of infinite integrals which were derived from a semi-infinite earth model.

The calculation of $\boldsymbol{Z_T}$ in buried cables is more significant than aerial lines. First, the self and mutual earth return impedances constitute more than two thirds of the series impedance matrix in buried cables. Second, the frequency dependent parameter $\boldsymbol{Z_T}$ has to be evaluated at many discrete points to obtain a good resolution of the transient response in the time domain. For instance, a transient analysis caused by switching operations in power systems with a typical frequency range from 1 Hz $\leq$ f $\leq$ 1 MHz may require 1024 samples of the spectrum. The example of power transmission system of buried cables depicted in Fig. 1, with n=3 buried cables and m=2 conductors per cable, requires to evaluate $\boldsymbol{Z_T}$ at least 1024 x 2/3 x $(mn)^2$ times. This fact is complicated due to the accurate evaluation of $\boldsymbol{Z_T}$ requires to solve Pollaczek's integral [2-7]. This integral does not have analytic solution and its numerical solution through generic integration routines in a conventional PC becomes time consuming. This is mainly due to the irregular and highly oscillatory behavior of its integrand. For decades, most of the research efforts to solve Pollaczek's integral have been focused on solutions based on approximated formulas [8-13]. The main drawback with approximated formulas is that most of them are valid within certain frequency ranges [4].

Between 1969 and 1973, Wedepohl and Wilcox published a very exhaustive analysis to solve the Pollaczek's integral [6-7]. The major contribution of these authors has been the decomposition of Pollaczeck's integral into a set of improper integrals plus a definite integral. The improper integrals were approximated via Bessel functions. Wedepohl and Wilcox derived also an infinite series solution to the definite integral. For many years, this series solution had been cumbersome to implement due to typographical errors. Cortez R. I. in [14] and Uribe-Campos F.A. in [15] have made some efforts to find and correct these typographical errors. These authors have successfully implemented the original Wedepohl and Wilcox's series solution for a limited frequency range and cable configurations. This paper uses the Wedepohl and Wilcox's analysis to derive an efficient and reliable algorithmic solution for solving the Pollaczek's integral. Through this algorithmic solution the earth return impedance can be evaluated accurately and efficiently for the broad range of applications published in the specialized literature.

II. Earth Return Impedance of Buried Cables

In 1926, Pollaczek published a set of improper integrals to evaluate the electromagnetic coupling caused by an infinite thin filament in the presence of an imperfect conducting soil [2-3].

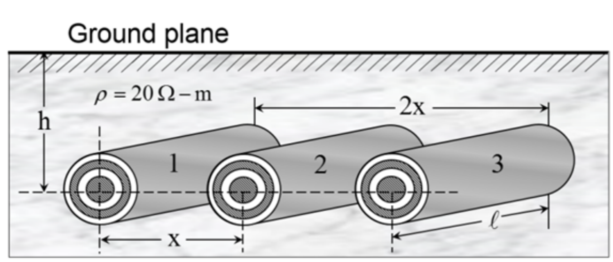

Fig. 1: Power transmission system of buried cables.

The work was supported by the National Council of Science and Technology of Mexico (CONACYT) and the Center for Research in Mathematics A.C. (CIMAT).

R. Iracheta and N. Flores-Guzmán are with the Department of Industrial Mathematics at the Center for Research in Mathematics A. C. (CIMAT), Guanajuato, GTO 36240, Mexico (e-mails: reynaldo.iracheta@cimat.mx and norberto@cimat.mx).

Paper submitted to the International Conference on Power Systems Transients (IPST2015) in Cavtat, Croatia June 15-18, 2015

The general formula derived by Pollaczek to evaluate the mutual impedance between two buried cables is given by:

$$\boldsymbol{Z_T} = \frac{\mathrm{j}\omega\mu_0}{2\pi}\int_{-\infty}^{\infty}\left[\begin{array}{l}\dfrac{\mathrm{e}^{-(\mathrm{h}_1+\mathrm{h}_2)\sqrt{\beta^2+(1/p^2)}}}{|\beta|+\sqrt{\beta^2+\left(1/p^2\right)}}\\ +\dfrac{\mathrm{e}^{-|\mathrm{h}_1-\mathrm{h}_2|\sqrt{\beta^2+(1/p^2)}}-\mathrm{e}^{-|\mathrm{h}_1+\mathrm{h}_2|\sqrt{\beta^2+(1/p^2)}}}{2\sqrt{\beta^2+\left(1/p^2\right)}}\end{array}\right]\mathrm{e}^{\mathrm{j}\beta x}\mathrm{d}\beta \quad (1\mathrm{a})$$

where ω is the angular frequency in rad/s, μ_0 ($\mu_0 = 4\pi \times 10^{-7}$ Wb/(A·m)) is to the magnetic permeability of the free space, β is the dummy variable, x is the horizontal distance between cables, h_1 and h_2 are the depths of cables 1 and 2 and $\boldsymbol{p} = \sqrt{\rho_{soil} / j\omega\mu_0}$ is the complex depth with the ground resistivity ρ_{soil}. This earth model assumes that $\mu_0 = \mu_{ground}$ and the soil is a homogeneous medium whose flat surface divides the space into two semi-infinite regions: soil and air.

The second term of (1a) can be approximated by

$$\boldsymbol{K_0}\left(\mathrm{d} / p\right) = \int_{-\infty}^{\infty}\frac{\mathrm{e}^{-|\mathrm{h}_1-\mathrm{h}_2|\sqrt{\beta^2+(1/p^2)}}}{2\sqrt{\beta^2+\left(1/p^2\right)}}\mathrm{e}^{\mathrm{j}\beta x}\mathrm{d}\beta \quad (2\mathrm{a})$$

and

$$\boldsymbol{K_0}\left(\mathrm{D} / p\right) = \int_{-\infty}^{\infty}\frac{\mathrm{e}^{-|\mathrm{h}_1+\mathrm{h}_2|\sqrt{\beta^2+(1/p^2)}}}{2\sqrt{\beta^2+\left(1/p^2\right)}}\mathrm{e}^{\mathrm{j}\beta x}\mathrm{d}\beta \quad (2\mathrm{b})$$

where $\boldsymbol{K_0}$ is the modified Bessel function of second type and order zero. Thus, by replacing (2a) and (2b) in in (1a) $\boldsymbol{Z_T}$ becomes:

$$\boldsymbol{Z_T} = \frac{\mathrm{j}\omega\mu_0}{2\pi}\left[\boldsymbol{K_0}\left(\mathrm{d} / \boldsymbol{p}\right) - \boldsymbol{K_0}\left(\mathrm{D} / \boldsymbol{p}\right) + \boldsymbol{J}\right] \quad (3\mathrm{a})$$

where $d = \sqrt{x^2 + \left(h_1 - h_2\right)^2}$ is the distance between cables 1 and 2, $\boldsymbol{p} = \sqrt{\rho_{soil} / j\omega\mu_0} = 0.5\sqrt{2\rho_{soil} / j\omega\mu_0}\left(1 - j\right)$ is the complex depth, $D = \sqrt{x^2 + \left(h_1 + h_2\right)^2}$ is the distance between a real cable and the image from the other one. Physical variables h_1, h_2, x, D and d and their geometric relationships are shown in Fig. 2. The remaining term $\boldsymbol{J}$ is the Pollaczek's integral

$$\boldsymbol{J} = \int_{-\infty}^{\infty}\frac{\mathrm{e}^{-(\mathrm{h}_1+\mathrm{h}_2)\sqrt{\beta^2+(1/\boldsymbol{p})^2}}}{|\beta| + \sqrt{\beta^2 + \left(1/\boldsymbol{p}^2\right)}}\mathrm{e}^{\mathrm{j}\beta x}\mathrm{d}\beta. \quad (3\mathrm{b})$$

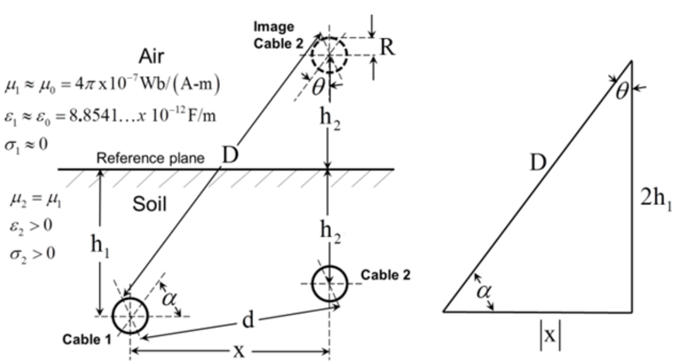

Fig. 2: System layout of buried cables with geometric relationships of physical variables.

It also should be noted that expressions (3a) and (3b) becomes the self-earth return impedance when x is the conductor radius R and $h_1 = h_2$.

In 1973, Wedepohl and Wilcox introduced the following analytical decomposition for (3b) [6-7]:

$$\boldsymbol{J} = \left[\begin{array}{l}\dfrac{4\mathrm{h}^2}{\mathrm{D}^2}\boldsymbol{K_0}\left(\mathrm{D} / \boldsymbol{p}\right)\\ +\dfrac{\left(4\mathrm{h}^2 - 2\mathrm{x}^2\right)\boldsymbol{p}}{\mathrm{D}^3}\left[\boldsymbol{K_1}\left(\mathrm{D} / \boldsymbol{p}\right) - \dfrac{\left(2\mathrm{h} + \boldsymbol{p}\right)}{\mathrm{D}}\mathrm{e}^{-\frac{2\mathrm{h}}{\boldsymbol{p}}}\right] - \boldsymbol{I}_{\mathrm{w}}\end{array}\right] \quad (3\mathrm{c})$$

with

$$\boldsymbol{I}_{\mathrm{w}} = -\frac{2\mathrm{h}|\mathrm{x}|}{\mathrm{D}^2}\int_{2\mathrm{h}/\mathrm{D}}^{1}\left(2\sqrt{1-\mathrm{t}^2} - \frac{1}{\sqrt{1-\mathrm{t}^2}}\right)\left(\mathrm{e}^{-\mathrm{D}t/p}\right)\mathrm{dt} \quad (3\mathrm{d})$$

and $\mathrm{h} = \left(\mathrm{h}_1 + \mathrm{h}_2\right) / 2$.

The modified Bessel functions $\boldsymbol{K_0}$ and $\boldsymbol{K_1}$ in (3c) evaluate improper integrals via convergent series. These Bessel functions are easy to compute in modern mathematical tools such as Matlab®. The second term in (3c) has an algebraic expression which does not present computational difficulties. The third term $\boldsymbol{I}_{\mathrm{w}}$ in (3c) is named in this paper the Wedephol-Wilcox´s integral. This integral does not have analytical solution but can be easily computed with any numerical integration method. In references [6-7], Wedepohl and Wilcox have derived an infinite series solution for solving $\boldsymbol{I}_{\mathrm{w}}$ which up to date is still awkward to implement for a broad range of frequencies and cable configurations. Uribe and Ramirez in [16] have implemented the original series solution published by Wedepohl and Wilcox as part of a hybrid algorithm to solve $\boldsymbol{I}_{\mathrm{w}}$ with an extended factor $|D/p| \leq 2$. Theodoulidis has also proposed in [17] the use of the special function 'hypergeometric' which is based on a series expansion for solving $\boldsymbol{I}_{\mathrm{w}}$. The author mentions that a maximum of 20 terms are enough to provide a good accuracy, however, the errors have not been assessed for all range of parameters. In Appendix A are provided the correct terms of the Wedepohl and Wilcox's series solution. Its accuracy has been assessed against the numerical integration method for a broad range of parameters.

Wedepohl and Wilcox have also proposed an approximated formula for calculating the earth return impedance $\boldsymbol{Z_T}$ on buried cables. However, the main disadvantage with this formulation is that its application range is also limited for low-frequency or by a factor $|D/p| \leq 1/4$.

III. Series Expansion Solution

The Taylor-series expansion method is derived from the Wedepohl-Wilcox's integral ($\boldsymbol{I}_{\mathrm{w}}$). For the analysis, let (3d) as

$$\boldsymbol{I}_{\mathrm{w}} = -\frac{2\mathrm{h}|\mathrm{x}|}{\mathrm{D}^2}\left[2\,\boldsymbol{I}_{\mathrm{w}1} - \boldsymbol{I}_{\mathrm{w}2}\right] \quad (4\mathrm{a})$$

where

$$\boldsymbol{I}_{\mathrm{w}1} = \int_{2\mathrm{h}/\mathrm{D}}^{1}\left(\sqrt{1-\mathrm{t}^2}\right)\left(\mathrm{e}^{-\mathrm{D}t/p}\right)\mathrm{dt} \quad (4\mathrm{b})$$

and

$$\boldsymbol{I}_{\mathrm{w}2} = \int_{2\mathrm{h}/\mathrm{D}}^{1}\left(\frac{1}{\sqrt{1-\mathrm{t}^2}}\right)\left(\mathrm{e}^{-\mathrm{D}t/p}\right)\mathrm{dt}. \quad (4\mathrm{c})$$

By replacing radical terms in (4b) and (4c) by

$$\sqrt{1-t^2}=\sum_{n=0}^{\infty}\left(-\frac{4^{-n}t^{2n}(2n)!}{(n!)^2(2n-1)}\right) \tag{5a}$$

and

$$\frac{1}{\sqrt{1-t^2}}=\sum_{n=0}^{\infty}\left(\frac{4^{-n}t^{2n}(2n)!}{(n!)^2}\right). \tag{5b}$$

Thus, the infinite series expansion for (4b) and (4c) is

$$\boldsymbol{I}_{w1}=-\sum_{n=0}^{\infty}\left(\frac{4^{-n}(2n)!}{(n!)^2(2n-1)}\int_{2h/D}^{1}t^{2n}e^{-Dt/p}dt\right) \tag{6a}$$

and

$$\boldsymbol{I}_{w2}=\sum_{n=0}^{\infty}\left(\frac{4^{-n}(2n)!}{(n!)^2}\int_{2h/D}^{1}t^{2n}e^{-Dt/p}dt\right). \tag{6b}$$

The definite integral in (6a) and (6b) can be evaluated analytically from the Whittaker M function **M**(a, b, z):

$$\int_{2h/D}^{1}t^{2n}e^{-Dt/p}dt=\left[\mathbf{C_1}\cdot\mathbf{M}(n,n+0.5,Dt/p)\right]_{2h/D}^{1} \tag{7a}$$

where

$$\mathbf{C}_1=\left(t^n(D/p)^{-(n+1)}e^{-0.5Dt/p}\right)/(2n+1) \tag{7b}$$

The Whittaker M function can also be defined in terms of a confluent hypergeometric function **F**(n, d, z):

$$\mathbf{M}(n,n+0.5,Dt/p)=e^{-0.5Dt/p}(Dt/p)^{n+1}\mathbf{F}(1,2(n+1),Dt/p). \tag{7c}$$

By replacing (7c) in (7a)

$$\int_{2h/D}^{1}t^{2n}e^{-Dt/p}dt=\left[\left(\frac{t^{2n+1}e^{-Dt/p}}{(2n+1)}\right)\cdot\mathbf{F}(1,2(n+1),Dt/p)\right]_{2h/D}^{1} \tag{7d}$$

where

$$\mathbf{F}(1,2(n+1),Dt/p)=\sum_{k=0}^{\infty}\left(\frac{\mathbf{C}_{1,k}}{\mathbf{C}_{2(n+1),k}}\cdot\frac{(Dt/p)^k}{k!}\right). \tag{7e}$$

$C_{1,k}$ and $C_{2(n+1),k}$ in (7e) are the ascending factorials which are given by

$$\mathbf{C}(1,k)=\frac{\Gamma(1+k)}{\Gamma(1)}=k! \tag{7f}$$

and

$$\mathbf{C}(2(n+1),k)=\frac{\Gamma(2n+2+k)}{\Gamma(2n+2)}=\frac{(2n+k+1)!}{(2n+1)!}. \tag{7g}$$

By replacing (7d) with definitions (7e), (7f) and (7g) in (6a) and (6b) and by truncating the resulting Taylor-series expansion at orders N and K, $\boldsymbol{I}_{w1}$ and $\boldsymbol{I}_{w2}$ become:

$$\boldsymbol{I}_{w1}=-\sum_{n=0}^{N}\left(\frac{4^{-n}(2n)!}{(n!)^2(2n-1)}\left[t^{2n+1}e^{-Dt/p}\sum_{k=0}^{K}\left(\frac{(2n)!\cdot(Dt/p)^k}{(2n+k+1)!}\right)\right]_{\frac{2h}{D}}^{1}\right) \tag{8a}$$

and

$$\boldsymbol{I}_{w2}=\sum_{n=0}^{N}\left(\frac{4^{-n}(2n)!}{(n!)^2}\left[t^{2n+1}e^{-Dt/p}\sum_{k=0}^{K}\left(\frac{(2n)!\cdot(Dt/p)^k}{(2n+k+1)!}\right)\right]_{\frac{2h}{D}}^{1}\right). \tag{8b}$$

By evaluating upper and lower limits of (8a) and (8b)

$$\boldsymbol{I}_{w1}=-\sum_{n=0}^{N}\left(\frac{4^{-n}(2n)!}{(n!)^2(2n-1)}\sum_{k=0}^{K}\frac{(2n)!}{(2n+k+1)!}\begin{pmatrix}e^{-Dt/p}\cdot(Dt/p)^k\\ -t^{2n+1}e^{-\frac{Dt}{p}}(Dt/p)^k\end{pmatrix}\right) \tag{9a}$$

and

$$\boldsymbol{I}_{w2}=\sum_{n=0}^{N}\left(\frac{4^{-n}(2n)!}{(n!)^2}\sum_{k=0}^{K}\frac{(2n)!}{(2n+k+1)!}\cdot\begin{pmatrix}e^{-D/p}(D/p)^k\\ -t^{2n+1}e^{-Dt/p}(Dt/p)^k\end{pmatrix}\right). \tag{9b}$$

The numerical solution for $\boldsymbol{I}_{w1}$ and $\boldsymbol{I}_{w2}$ can be done efficiently by assuming the following considerations:

a) A loop of length N is used to compute the first summation in (9a) and (9b),

b) Terms $e^{-D/p}$ $(D/p)^k$ and $e^{-D/p}(Dt/p)^k$ are defined as constant vectors. These expressions contains the frequency dependence of the earth return parameter,

c) Factorial expressions $F_1 = 4^{-n}(2n)!/((n!)^2(2n-1))$ in (9a) and $F_2 = 4^{-n}(2n)!/((n!)^2)$ in (9b) are solved recursively to overcome overflows when large factorials are computed. The code for this recursive algorithm is provided in Appendix B. Additionally, the sum of these factorial expressions are depicted in Figs. 3a and 3b. It can be observed from Fig. 3a that the sum of the first factorial expression in (9a) decreases rapidly for N = 10 iterations reaching values below to 0.01. As opposite, the sum of the first factorial expression in (9b) decreases slowly and thus, larger values of N are required to reach values below to 0.01. However, the following criterion can be used to truncate the series expansion in (9b) for small values of N when t < 1:

$$\boldsymbol{I}_{w2}=\boldsymbol{I}_{w2}+\frac{4^{-N}(2N)!}{(N!)^2}e^{-D/p}. \tag{9c}$$

d) The second summation in (9a) and (9b) with the factorial term $F_3= (2n)!/(2n+k+1)!$ is also solved recursively in a vectorized manner as described in Appendix B. The plot of this summation is depicted in Fig. 2c for $|D/p|=1$, K=20, and t=0. It can be observed that the sum reaches values below to 0.01 for N ≤ 20 iterations.

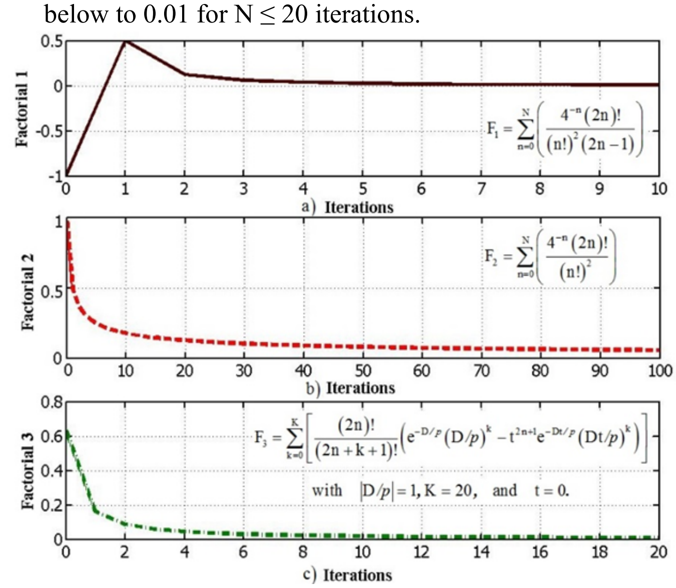

Fig. 3: Solution of factorial expressions for different values of n. a) Factorial F_1, b) Factorial F_2 and c) Factorial F_3.

IV. Convergence, Accuracy and Stability

The series expansion method for $\boldsymbol{I}_w$, described in the previous section as function of physical and electrical variables (h, x, D, ω, σ and p), is now evaluated for a broad range of parameters to test its accuracy. For doing this, the next dimensionless variables are introduced

$$\mathrm{D}/p, \quad t = 2h/\mathrm{D}, \quad \text{and} \quad \eta = \frac{x}{2h}. \qquad (10a)$$

Dimensionless variables relate physical and electrical variables. Table I provides the range of values for physical and electrical variables [18]. These values are used to establish the range of most practical interest for dimensionless parameters (10a) which are provided in Table II.

The series expansion is applied to solve $\boldsymbol{I}_w$ for values $|\mathrm{D}/p| \leq 60$ and 0 $10^{-3} \leq \eta \leq 10^{3}$. For this test, the values used for σ = 0.05 S/m and the frequency range has been uniformly sampled from 1 Hz to 1 MHz. Figs. 4a and 4b provide the results in the form of 3D graphs for the real and imaginary components for $\boldsymbol{I}_w$. The figures were generated by solving $\boldsymbol{I}_w$ 1300 times with N = 20 iterations. The computational task required for doing this task by an Intel® Core™ i7-3770 CPU @ 3.40 GHz running MATLAB® V. 7.14 was less than 1 s.

The numerical quadrature Gauss-Lobatto integration method "quadl" is also applied to solve $\boldsymbol{I}_w$ for the same values described above. The results obtained with the numerical integration are compared against the series algorithm through the absolute percent error (ε),

$$\varepsilon = 100 \cdot \left(\boldsymbol{I}_{w,\text{series}} - \boldsymbol{I}_{w,\text{integration}} \right) \qquad (10b)$$

Absolute percent errors obtained from the broad range simulation are depicted in Fig. 4c. It can be observed that magnitudes of errors are always below to 0.15%.

Table III provides information regarding to the number iterations, convergence and stability of the proposed series solution. The results provided in this table were calculated by using a factor $|\mathrm{D}/p| = 3$ and K = 150 for computing the second sum in (9a) and (9b). The fourth column of Table IV provides the maximum errors (ε_{max}) for different number of iterations. It is observed that ε decreases rapidly as N increase. So that, the convergence and stability for the series solution is guaranteed when ε tends to zero.

The criterion to truncate the series at order N is

$$|\boldsymbol{I}_{w,\text{series}}| \leq \varepsilon.$$

TABLE I
Physical Variables

0.1	≤ h ≤	10^2	[m]
2 π	≤ ω ≤	2 π x 10^6	[rad/s]
10^{-4}	≤ σ ≤	1	[S/m]
10^{-2}	≤ x ≤	10^3	[m]

TABLE II
Dimensionless Parameters

10^{-5}	≤ |D/p| ≤	10^3
10^{-3}	≤ η ≤	10^3

By assuming ε = 0.015, the number of iterations required to truncate the Taylor-series expansion is N = 20 iterations. This is the practical limit recommended for the authors to perform electromagnetic transient studies.

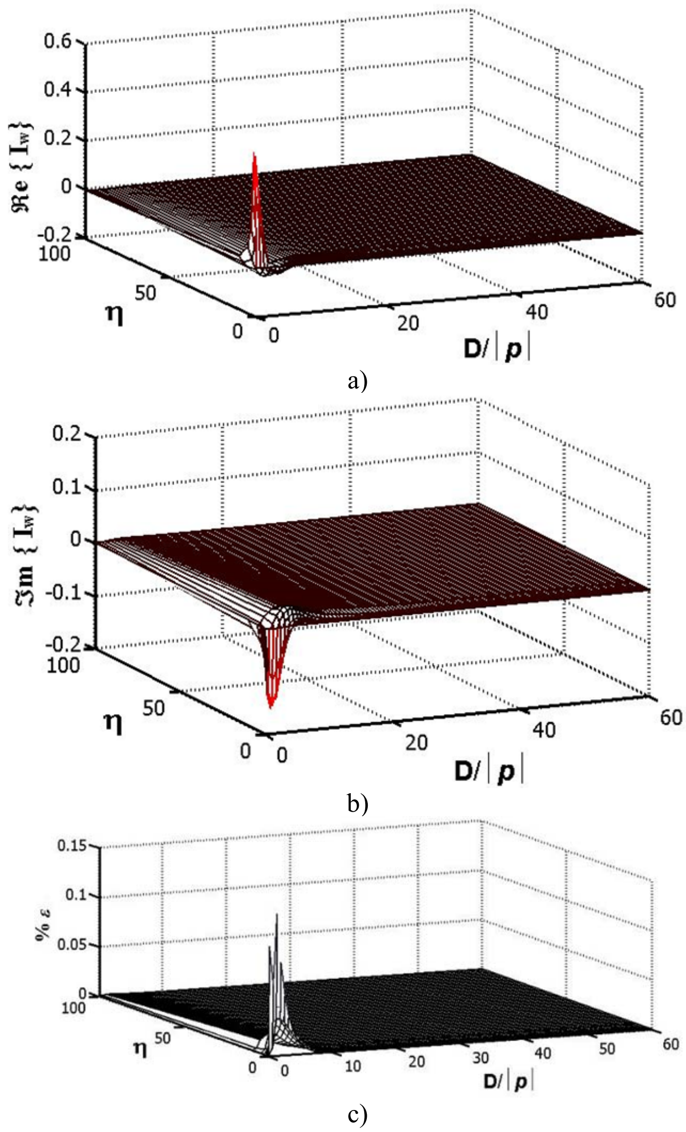

Fig. 4. $\boldsymbol{I}_w$ solution for η as shown in Table II and $|\mathrm{D}/p| \leq 60$. a) Real part of $\boldsymbol{I}_w$, b) Imaginary part of $\boldsymbol{I}_w$ and c) Absolute percent error.

TABLE III
Analysis of Convergence and Stability for $\boldsymbol{I}_{w,\text{ series}}$

# ITER N	FACTOR |D/p|	FACTOR K	MAX. ERROR (% ε)
1	3	150	0.9312
3	3	150	0.2417
5	3	150	0.1183
10	3	150	0.04325
15	3	150	0.02377
20	**3**	**150**	**0.01500**
30	3	150	0.00848
40	3	150	0.00552

IV. STUDY CASES

The self and mutual earth return impedances ($\mathbf{Z}_T$) are evaluated with three different methods: a) the Taylor-series expansion method proposed in this paper, b) the numerical integration method "quadl" [19], and c) the closed formula published by Saad, Gaba and Giroux [9]. The validation test consists in to compare the frequency responses for $\mathbf{Z}_T$ obtained with the aforementioned methods through the absolute percent error. It should be pointed out that numerical integration method is applied for both, the Pollaczek´s integral (3b) and the Wedepohl´s integral (4a). The solution of (3c) with the numerical integration is considered the reference case for doing these comparisons.

A) Typical case of a power system of buried cables

A power system of three buried cables such as the one depicted in Fig. 1 is used as to perform the validation test. The physical variables for this system are shown in the transversal layout of Fig. 5. This example corresponds to the benchmark case published by Wedepohl and Wilcox in 1973.

Figs. 6 and 7 show plots of self and mutual impedances (Z_T) in terms of their magnitudes in per unit length (Ω/m) and angles in degrees. These frequency responses were calculated with N=20 iterations for the series algorithm and a tolerance of 10e-6 for the numerical integration. The accuracy of the results was measured through the criterion of absolute percent error. By comparing absolute percent errors in Figs. 6 and 7 one can say that Saad-Gaba-Giroux formula gives significant errors greater than 1% at high frequency. As opposite, the series expansion and the numerical integration give accurate results, smaller than 0.1 %, over all the entire frequency range. The numerical integration is slightly more accurate than the series algorithm. This is due to the series algorithm is truncated at N = 20 iterations.

B) Case of AC interference on oil and gas pipelines

There are practical cases in which oil, gas and water pipelines share the same right of way with power transmission system of aerial lines and buried cables. These cases are the main of concern for public utilities due to high voltage in power lines and cables can cause AC interference on these pipelines. For instance, during normal operation conditions power transmission systems induce voltages and currents between their conductors and any other surrounding conducting material in the vicinity. The magnitudes of induced voltages and currents can be greater during abnormal conditions caused by strike lighting and faults. Part of this energy can be captured by the pipelines and transported along its entire length to the gas stations or water supply valves where can result in an electrical hazard for people touching the pipelines or metallic structures connected to the pipeline or simply standing nearby. Furthermore, the AC interference can also result in damage to the pipeline and its coating. To predict and mitigate these conditions, it is necessary to count with tools for the accurate evaluation of earth return impedance.

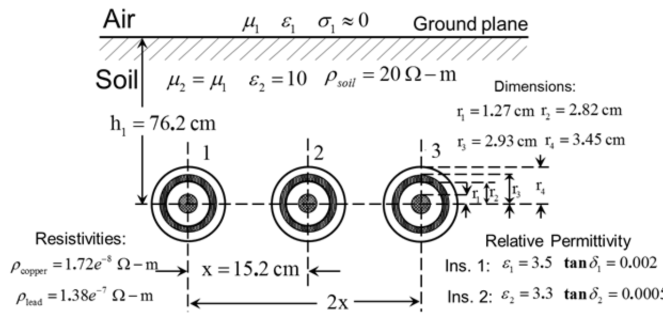

Fig. 5: System layout of buried cables.

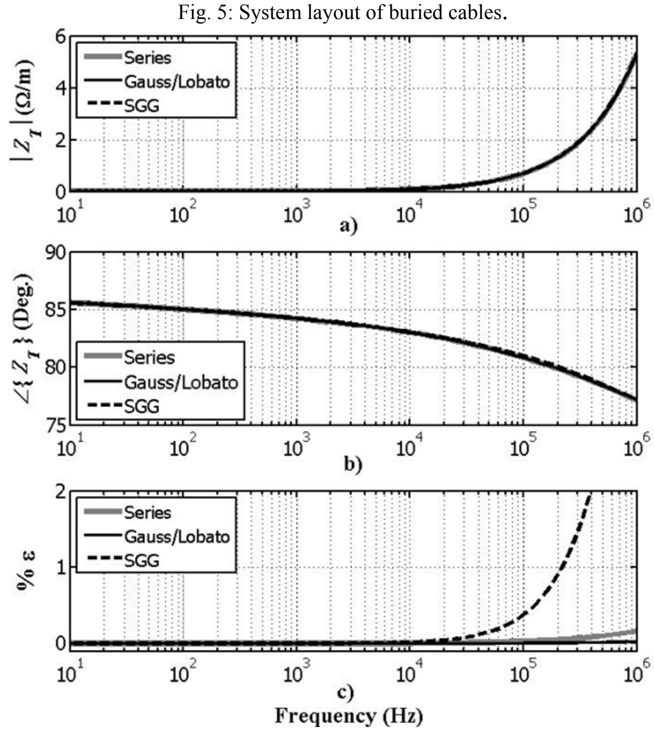

Fig. 6: Self $\mathbf{Z}_T$ for a buried conductor. a) Magnitude $|\mathbf{Z}_T|$ (Ω/m), b) Angle of $|\mathbf{Z}_T|$ (Deg.) and c) Absolute percent errors.

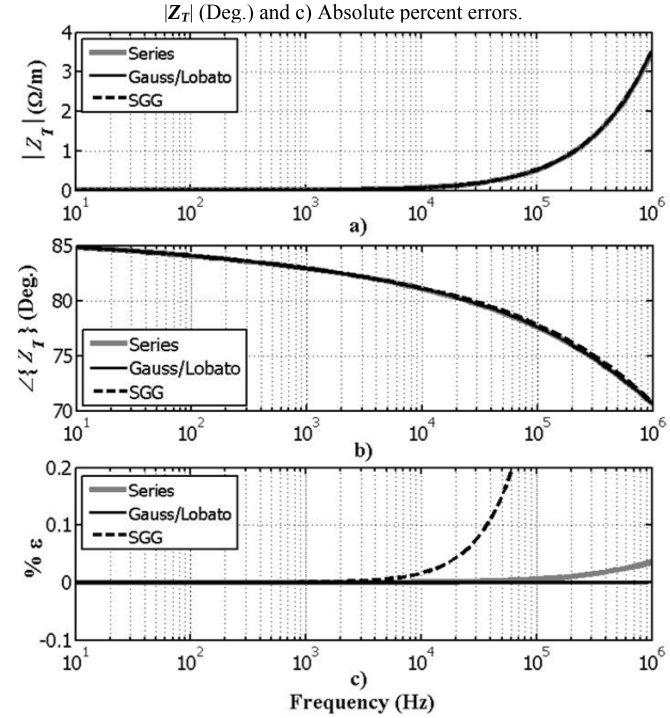

Fig. 7: Mutual $\mathbf{Z}_T$ for a buried conductor. a) Magnitude $|\mathbf{Z}_T|$ (Ω/m), b) Angle of $|\mathbf{Z}_T|$ (Deg.) and c) Absolute percent errors.

Let us consider the power transmission of buried cables shown in Fig. 8 which is electromagnetically coupled to a petroleum/gas pipeline. The ground resistivity is 20 Ω-m. For the calculation of mutual electromagnetic couplings between conductors 3 and 4 consider a horizontal distance of 30 meters and a depth of 0.762 m for both conductors.

Fig. 9 shows the self and mutual impedance ($\boldsymbol{Z_T}$) plots as function of frequency in terms of its magnitude in per unit length (Ω/m) and angle in degrees. For this case, the frequency range has been logarithmically spaced from 10 Hz to 1 MHz by using 100 points per decade. Frequency responses for Z_T have been calculated with the series solution method proposed in this paper, the Gauss-Lobatto numerical integration and the Saad-Gaba-Giroux formulation [9]. By comparing the three methods used one can say that Saad-Gaba-Giroux gives significant errors at high frequency. In contrast, the Taylor-series expansion method and the Gauss-Lobatto numerical integration give the same accuracy over all the entire frequency range. However, the main advantage of the series solution regarding to Gauss-Lobatto is its low computational demanding. Table V provides the computational time required for both methods with an Intel® Core™ i7-3770 CPU @ 3.40 GHz running MATLAB® V. 7.14. It can be observed that the series solution is faster than the numerical integration method.

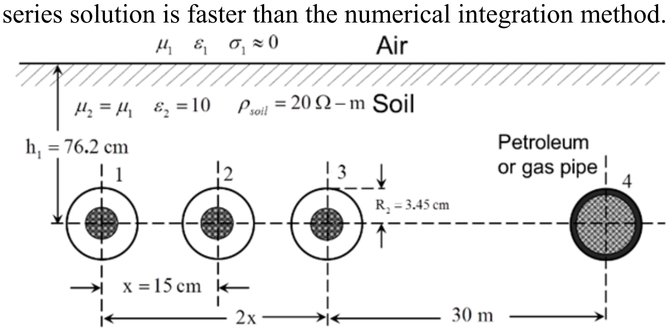

Fig. 8: Transversal layout with an oil gas pipe.

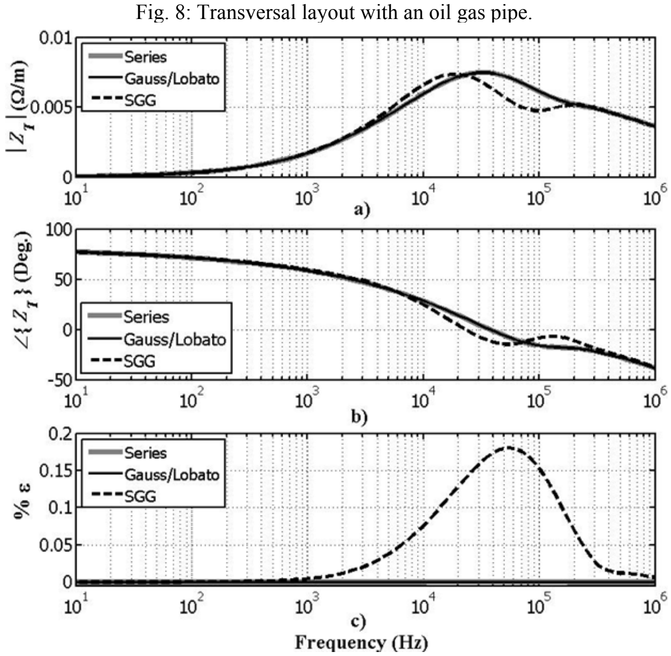

Fig.9: Mutual $\boldsymbol{Z_T}$ for a buried conductor. a) Magnitude $|\boldsymbol{Z_T}|$ (Ω/m), b) Angle. of $|\boldsymbol{Z_T}|$ (Deg.) and c) Absolute percent errors.

TABLE IV
COMPUTATIONAL TIME

Method		Time (s)
Series	N =20 iterations	0.0781
Gauss-Lobatto	Tolerance = 10^{-9}	0.9219

V. TRANSIENT STUDY

The inverse Numerical Laplace Transform (NLT) technique based on the frequency domain is used as reference to calculate the transient response of an open circuit test [20]. The Taylor-Series expansion method and the numerical integration have been incorporated into the CABLE toolbox of the NLT technique for evaluating the frequency-dependent parameter $\boldsymbol{Z_T}$. The open circuit transient response is calculated with the real-time platform RSCAD/RTDS®. The CABLE program has been adjusted to evaluate $\boldsymbol{Z_T}$ with the numerical integration and the transient calculation with the full frequency dependent cable model. The aim of this section is to compare the transient responses obtained with NLT and the commercial real-time platform RSCAD/RTDS®.

Consider the three-phase underground power system benchmark proposed by Wedepohl and Wilcox in 1973. The data for this system is provided in Fig. 5. Each underground cable is made up by a core and a screen with an insulator between them. The core is the main electric conductor while the sheath is its mechanical protection.

A) Open circuit test

A unit step voltage of 1 p.u. is applied at t = 0 s to the core of cable 1 as shown in Fig. 10. At the sending end, cores of cables 2 and 3 are left in open circuit while sheaths are short-circuited. At the receiving end, all conductors are left open. The time step to perform this simulation test is 10 μs due to it is the minimum allowed by RSCAD/RTDS® with the frequency-dependent model. The NLT technique uses an observation time of 3 ms with N = 1000 samples to match the simulation time-step.

The voltage transient response at the receiving end to the energized core of cable 1 is depicted in Fig. 11a while induced voltages for cores 2 and 3, and sheaths 1, 2 and 3 are depicted in Fig. 11b. The open circuit transient responses obtained through the inverse NLT technique with the Taylor-Series expansion and the numerical integration match exactly the same behavior. Absolute errors among these waveforms are less than 10^{-4}. However, voltage waveforms captured from the real-time simulation in RTDS presents some small discrepancies with the NLT technique. These small differences are probably due to larger time steps do not represent the full frequency dependence of parameters. For instance, a time-step of 10 μs corresponds to an effective bandwidth of 15 kHz. To have a good resolution of the transient response in the time domain it is necessary to perform the simulation with time-steps smaller than 10 μs.

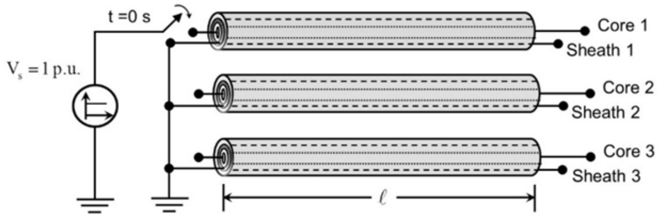

Fig. 10: Cable system connection diagram.

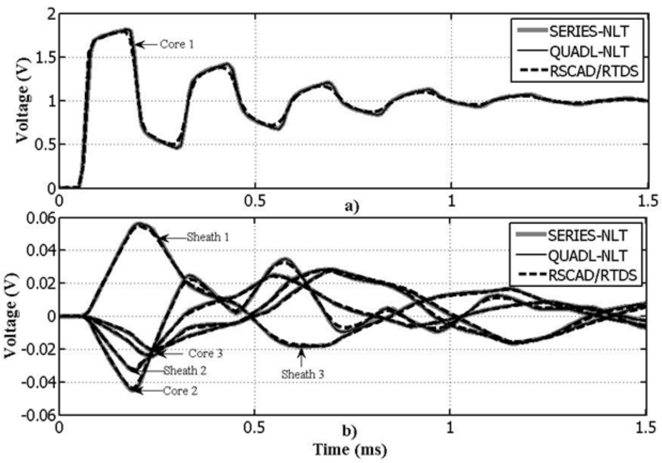

Fig. 11: Voltage transient responses at the receiving end, a) Energized core of cable 1, b) Induced conductors at cores 2, 3 and sheaths 1, 2, 3.

VI. Conclusions

A numerical solution method based on a Taylor-series expansion has been presented to evaluate the earth return impedance in buried cables. It has been demonstrated that this method provides enough accuracy for the broad range of application cases published in the specialized literature. Its execution in a conventional PC is always faster than the numerical integration method. This reliable method can be used to be incorporated in CABLE routines of electromagnetic transients programs such as the NLT technique and the real-time platform RSCAD/RTDS®.

VII. Appendix A

The Wedepohl and Wilcox's series solution can be split up into the following four types of terms:

$$\boldsymbol{S}_w\left(\mathrm{D}/p,\mathrm{x},\mathrm{h}\right)=\boldsymbol{S}_{w1}-\boldsymbol{S}_{w2}-\boldsymbol{S}_{w3}+\boldsymbol{S}_{w4} \qquad (\mathrm{A}.1)$$

where

$$\boldsymbol{S}_{w1}=\boldsymbol{[}\left\{\theta-\frac{2\mathrm{h}|\mathrm{x}|}{\mathrm{D}^2}\right\}$$
$$+\frac{1}{2(2!)}\left(\frac{\mathrm{D}}{\boldsymbol{p}}\right)^2\left\{\frac{(2\mathrm{h})|\mathrm{x}|^3}{\mathrm{D}^4}+\frac{1}{2}\left(\theta-\frac{2\mathrm{h}|\mathrm{x}|}{\mathrm{D}^2}\right)\right\}$$
$$+\frac{1}{3(4!)}\left(\frac{\mathrm{D}}{\boldsymbol{p}}\right)^4\left\{\frac{(2\mathrm{h})^3|\mathrm{x}|^3}{\mathrm{D}^6}+\frac{3}{4}\left\{\frac{(2\mathrm{h})|\mathrm{x}|^3}{\mathrm{D}^4}+\frac{1}{2}\left(\theta-\frac{2\mathrm{h}|\mathrm{x}|}{\mathrm{D}^2}\right)\right\}\right\} \qquad (\mathrm{A}.2)$$
$$+\frac{1}{4(6!)}\left(\frac{\mathrm{D}}{\boldsymbol{p}}\right)^6\left\{\frac{(2\mathrm{h})^5|\mathrm{x}|^3}{\mathrm{D}^8}+\frac{5}{6}\left\{\frac{(2\mathrm{h})^3|\mathrm{x}|^3}{\mathrm{D}^6}+\frac{3}{4}\left\{\frac{(2\mathrm{h})|\mathrm{x}|^3}{\mathrm{D}^4}+\frac{1}{2}\left(\theta-\frac{2\mathrm{h}|\mathrm{x}|}{\mathrm{D}^2}\right)\right\}\right\}\right\}+\boldsymbol{...]}$$

$$\boldsymbol{S}_{w2}=\boldsymbol{[}-\left\{\frac{2}{3(1!)}\left(\frac{\mathrm{D}}{\boldsymbol{p}}\right)\left(\frac{|\mathrm{x}|^3}{\mathrm{D}^3}\right)\right\}$$
$$-\frac{2}{5(3!)}\left(\frac{\mathrm{D}}{\boldsymbol{p}}\right)^3\left\{\frac{(2\mathrm{h})^2|\mathrm{x}|^3}{\mathrm{D}^5}+\frac{2}{3}\left(\frac{|\mathrm{x}|^3}{\mathrm{D}^3}\right)\right\}$$
$$-\frac{2}{7(5!)}\left(\frac{\mathrm{D}}{\boldsymbol{p}}\right)^5\left\{\frac{(2\mathrm{h})^4|\mathrm{x}|^3}{\mathrm{D}^7}+\frac{4}{5}\left\{\frac{(2\mathrm{h})^2|\mathrm{x}|^3}{\mathrm{D}^5}+\frac{2}{3}\left(\frac{|\mathrm{x}|^3}{\mathrm{D}^3}\right)\right\}\right\} \qquad (\mathrm{A}.2)$$
$$-\frac{2}{9(7!)}\left(\frac{\mathrm{D}}{\boldsymbol{p}}\right)^7\left\{\frac{(2\mathrm{h})^6|\mathrm{x}|^3}{\mathrm{D}^9}+\frac{6}{7}\left\{\frac{(2\mathrm{h})^4|\mathrm{x}|^3}{\mathrm{D}^7}+\frac{4}{5}\left\{\frac{(2\mathrm{h})^2|\mathrm{x}|^3}{\mathrm{D}^5}+\frac{2}{3}\left(\frac{|\mathrm{x}|^3}{\mathrm{D}^3}\right)\right\}\right\}\right\}+\boldsymbol{...]}$$

$$\boldsymbol{S}_{w3}=\boldsymbol{[}\ -\{\theta\}$$
$$-\frac{1}{2(2!)}\left(\frac{\mathrm{D}}{\boldsymbol{p}}\right)^2\left\{\frac{(2\mathrm{h})|\mathrm{x}|}{\mathrm{D}^2}+\theta\right\}$$
$$-\frac{1}{4(4!)}\left(\frac{\mathrm{D}}{\boldsymbol{p}}\right)^4\left\{\frac{(2\mathrm{h})^3|\mathrm{x}|}{\mathrm{D}^4}+\frac{3}{2}\left\{\frac{(2\mathrm{h})|\mathrm{x}|}{\mathrm{D}^2}+\theta\right\}\right\} \qquad (\mathrm{A}.3)$$
$$-\frac{1}{6(6!)}\left(\frac{\mathrm{D}}{\boldsymbol{p}}\right)^6\left\{\frac{(2\mathrm{h})^5|\mathrm{x}|}{\mathrm{D}^6}+\frac{5}{3}\left\{\frac{(2\mathrm{h})^3|\mathrm{x}|}{\mathrm{D}^4}+\frac{3}{2}\left\{\frac{(2\mathrm{h})|\mathrm{x}|}{\mathrm{D}^2}+\theta\right\}\right\}\right\}+\boldsymbol{...]}$$

$$\boldsymbol{S}_{w4}=\boldsymbol{[}\frac{1}{1!}\left(\frac{\mathrm{D}}{\boldsymbol{p}}\right)\left\{\frac{|\mathrm{x}|}{\mathrm{D}}\right\}$$
$$+\frac{1}{3(3!)}\left(\frac{\mathrm{D}}{\boldsymbol{p}}\right)^3\left\{\frac{(2\mathrm{h})^2|\mathrm{x}|}{\mathrm{D}^3}+\frac{2}{1}\left\{\frac{|\mathrm{x}|}{\mathrm{D}}\right\}\right\}$$
$$+\frac{1}{5(5!)}\left(\frac{\mathrm{D}}{\boldsymbol{p}}\right)^5\left\{\frac{(2\mathrm{h})^4|\mathrm{x}|}{\mathrm{D}^5}+\frac{4}{3}\left\{\frac{(2\mathrm{h})^2|\mathrm{x}|}{\mathrm{D}^3}+\frac{2}{1}\left\{\frac{|\mathrm{x}|}{\mathrm{D}}\right\}\right\}\right\} \qquad (\mathrm{A}.4)$$
$$+\frac{1}{7(7!)}\left(\frac{\mathrm{D}}{\boldsymbol{p}}\right)^7\left\{\frac{(2\mathrm{h})^6|\mathrm{x}|}{\mathrm{D}^7}+\frac{6}{5}\left\{\frac{(2\mathrm{h})^4|\mathrm{x}|}{\mathrm{D}^5}+\frac{4}{3}\left\{\frac{(2\mathrm{h})^2|\mathrm{x}|}{\mathrm{D}^3}+\frac{2}{1}\left\{\frac{|\mathrm{x}|}{\mathrm{D}}\right\}\right\}\right\}\right\}+\boldsymbol{...]}$$

Fig. 12 shows the absolute percent errors obtained from a broad range simulation of A.1. It can be observed through this simulation that the application range of the Wedepohl and Wilcox's series solution is limited to small values of $|\mathrm{D}/p|$. Uribe and Ramirez in [16] have used a factor $|\mathrm{D}/p| \leq 2$.

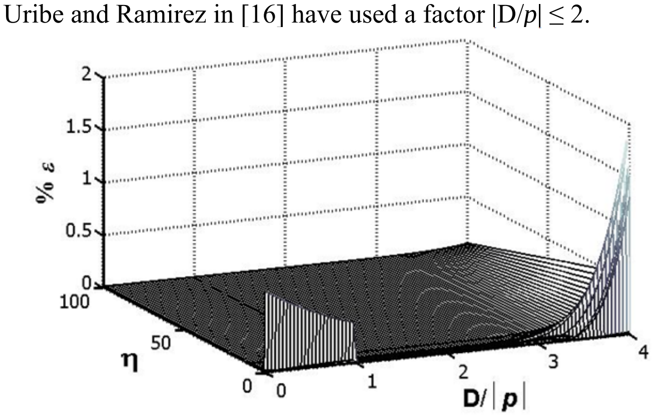

Fig. 12: Absolute percent errors for a broad range simulation of the Wedepohl and Wilcox's series solution.

VIII. Appendix B

The Matlab® code used in this paper to compute the series expansion method for both $\boldsymbol{I}_{w1}$ and $\boldsymbol{I}_{w2}$ is described below.

```
function [IW IW1 IW2] = series(N,K,DP,t)

% Inputs:
% N= Upper bound for computing the first summation;
% K= Upper bound for computing the second summation;
% DP= Constant defined in (10a);
% t= Dimensionless variable t=2h/D;
```

```
% Outputs:
% IW  = Numerical solution of (4a);
% IW1 = Numerical solution of (4b);
% IW2 = Numerical solution of (4c);

% Initialization:
IW=0; IW1=0; IW2=0;
% Constants:
DPT=DP*(t);
% Vectors:
CTE1= exp(-DP).*(DP).^(0:K);
CTE2= exp(-DPT).*(DPT).^(0:K);
% Constant Vector:
FA=1./factorial(0:K+1);

% Loop:
for n=0:N
    if n==0
       alfa= K;        % Constant
       F2=1;F1=-F2;   % Constant
    else
       a0= a0+1;
       a1=FA(end)/a0;
       a2=a1/(alfa+1);
       FA=((2*n-1)*(2*n))*([FA(3:end) a1 a2]);
       if n==1
               F2=2*4^(-n);F1=F2;
       else
               F2=(2*n-1)*F2/(2*n);
               F1=F2/(2*n-1);
       end
    end
    LS  = CTE1;
    LI  = t^(2*n+1)*CTE2;
    F3 = sum(FA.*(LS-LI));
    IW1 = IW1 – F3*F1;
    IW2 = IW2 + F2;
end
    if t<1
        WS2 = WS2+FAC/exp(DP);  % Eq. (9c)
    end
IW = -2h|x|(2*IW2-IW1)/D²;       % Eq. (4a)
```

The numerical computation of (4a) can also be illustrated as shown in the flowchart of Fig. 13.

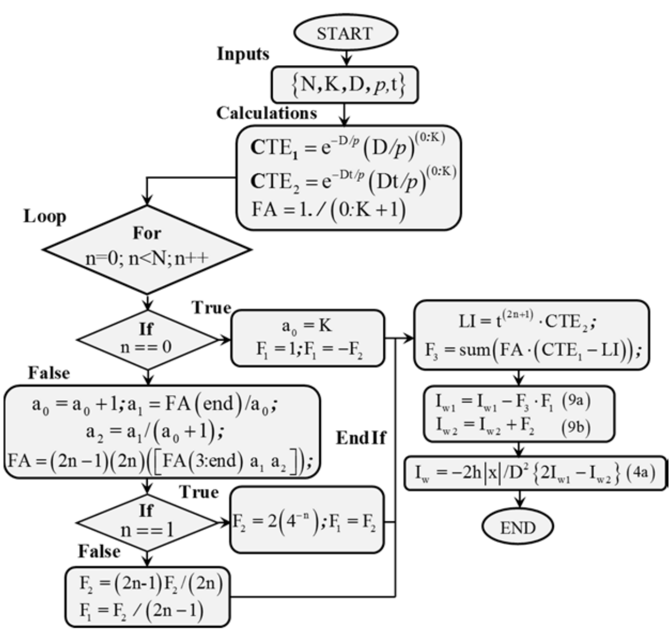

Fig. 13: Flowchart to compute the series expansions $\boldsymbol{I}_{w1}$ and $\boldsymbol{I}_{w2}$.

IX. Acknowledgment

The authors gratefully acknowledge the financial support to the National Council of Science and Technology of Mexico (CONACYT) and the Center for Research in Mathematics A.C. (CIMAT).

X. References

[1] J. Carson. "Wave Propagation in Overhead Wires with Ground Return", Bell System Technical Journal, Vol. 5, no. 4, pp. 539-554, 1926.

[2] F. Pollaczek, "Über das Feld einer unendlich langen wechsel stromdurchflossenen Einfachleitung", Electrische Nachrichten Technik, Vol. 3, No. 9, pp. 339-360, 1926.

[3] H. W. Dommel, Electromagnetic Transients Program Reference Manual (EMTP Theory Book), Prepared for Bonneville Power Administration, P.O. Box 3621, Portland, Ore., 97208, USA, 1986.

[4] F. A. Uribe, J. L. Naredo, P. Moreno and L. Guardado, "Electromagnetic Transients in Underground Transmission Systems Trough The Numerical Laplace Transform", Elsevier Science Ltd, Electrical Power and Energy Systems, 24 (2002), pp. 215-221.

[5] J. R. Marti, "Accurate Modeling of Frequency-Dependent Transmission Lines in Electromagnetic Transient Simulations." IEEE Transactions on Power Apparatus and Systems, Vol. PAS-101, pp. 147-157, 1982.

[6] D. J. Wilcox, Transient and Harmonic Induction in Underground Cable Systems, PhD. Thesis, The Victoria University of Manchester, Institute of Science and Technology, 1969.

[7] L. M. Wedepohl and D.J. Wilcox, "Transient analysis of underground power transmission systems", Proceedings of the IEE, Vol. 120, No. 2, February 1973.

[8] A. Ametani, "A general formulation of impedance and admittance of cables", IEEE Transactions on Power Apparatus Systems, Vol. PAS-99, No.3, pp. 902-910, May/June 1980.

[9] O. Saad, G. Gaba, M. Giroux, "A closed-form approximation for ground return impedance of underground cables", IEEE Transactions on Power Delivery, vol.11, No.3, pp. 1536-1545, July 1996.

[10] A. Semlyen, disscussion to "Overhead line parameters from handbook formulas and computer programs", by H. Dommel, IEEE Trans. on Power Apparatus and Systems, Vol. PAS-104, pp. 371, Feb 1985.

[11] A. Deri, G. Tevan, A. Semlyen and A. Castanheira, "The complex ground return plane: A simplified model for homogeneous and multi-layer earth return", IEEE Transactions on Power Apparatus and Systems, Vol. PAS-100, No. 8, pp. 3686-3693, August 1981.

[12] C. Gary, "Approche compléte de la propagation multifilaire en haute fréquence par utilisation des matrices compléxes", E.D.F Bulletin de la Direction des Études et Recherches, série B, No. 3/4, pp.5-20, 1976.

[13] C. Dubanton, "Calcul approaché des parametrés primaires et secondaires d'une ligne de transport –Valeurs homopolaires", E. D. F., Bulletin de la Direction des Études et Recherchches No. 1, sere B, 1969.

[14] Cortez, R. I., "Electromagnetic Modelling on Underground Cables (Spanish)", *Ingenierías*, 2009, vol. 12, no 44, p. 9.

[15] Uribe-Campos, F. A. "Numerical Infinite Series Solution of the Ground-Return Pollaczek Integral". Ingeniería Investigación y Tecnología, 2015, vol. 16, no 1.

[16] Uribe, F.A.; Ramirez, A., "Alternative Series-Based Solution to Approximate Pollaczek's Integral," Power Delivery, IEEE Transactions on, vol.27, no.4, pp.2425, 2427, Oct. 2012.

[17] Theodoulidis, T., "Exact Solution of Pollaczek's Integral for Evaluation of Earth-Return Impedance for Underground Conductors," Electromagnetic Compatibility, IEEE Transactions on, vol.54, no.4, pp.806,814, Aug. 2012.

[18] F. A. Uribe, J. L. Naredo, P. Moreno and L. Guardado, "Algorithmic evaluation of underground cable earth impedances," IEEE Transactions on Power Delivery, Vol. 19, No.1, pp.316-322, January 2004.

[19] W. Gander and W. Gautschi, "Adaptive Quadrature – Revisited", BIT, vol. 40, pp. 84-101, 2000.

[20] F. A. Uribe, J. L. Naredo, P. Moreno and L. Guardado, "Electromagnetic Transients in Underground Transmission Systems Through the Numerical Laplace Transform", Elsevier Science Ltd, Electrical Power and Energy Systems, 24 (2002), pp. 215-221.